

Robust Pedestrian Attribute Recognition Using Group Sparsity for Occlusion Videos

Geonu Lee^a, Kimin Yun^b, Jungchan Cho^{a,*}

^a*College of Information Technology, Gachon University, 1342 Seongnamdaero, Sujeong-gu, Sengnam-si, Gyeonggi-do, South Korea*

^b*Artificial Intelligence Research Laboratory, Electronics and Telecommunications Research Institute, 218 Gajeong-ro, Yuseong-gu, Daejeon, South Korea*

Abstract

Occlusion processing is a key issue in pedestrian attribute recognition (PAR). Nevertheless, several existing video-based PAR methods have not yet considered occlusion handling in depth. In this paper, we formulate finding non-occluded frames as sparsity-based temporal attention of a crowded video. In this manner, a model is guided not to pay attention to the occluded frame. However, temporal sparsity cannot include a correlation between attributes when occlusion occurs. For example, “boots” and “shoe color” cannot be recognized when the foot is invisible. To solve the uncorrelated attention issue, we also propose a novel group sparsity-based temporal attention module. Group sparsity is applied across attention weights in correlated attributes. Thus, attention weights in a group are forced to pay attention to the same frames. Experimental results showed that the proposed method achieved a higher F_1 -score than the state-of-the-art methods on

*Corresponding author

Email addresses: lkw3139@gachon.ac.kr (Geonu Lee), kimin.yun@etri.re.kr (Kimin Yun), thinkai@gachon.ac.kr (Jungchan Cho)

two video-based PAR datasets and five occlusion scenarios.

Keywords: Deep learning, Video-based pedestrian attribute recognition, Group sparsity loss, Temporal attention module

1. Introduction

Pedestrian attribute recognition (PAR) is a task that predicts various attributes of pedestrians detected by surveillance cameras. It is a human-searchable semantic description and can be used in soft biometrics for visual surveillance [1]. There have been several studies on this subject [2, 3, 4, 5, 6, 7, 8, 9] because of the importance of its applications, such as finding missing persons and criminals. However, the occlusion problem is still under-handled.

Because other objects and persons cause occlusions on a pedestrian, it is impossible to resolve it based on a single image. However, a video contains more information about a pedestrian than compared to an image, allowing a model to leverage information from multiple frames. Let us imagine that the lower body of a pedestrian is occluded at some frames, but the other frames have a visible lower-body appearance, as shown in Figure 2. In this case, we must use only the information from the frame with the lower body visible rather than the one in which the lower body is occluded. Recently, Chen *et al.* [10] proposed a video-based PAR method that calculates temporal attention probabilities to focus on frames that are important for attribute recognition. However, this method concentrates on incorrect frames if a pedestrian is occluded by other objects or other people. We argue that recent studies have not yet considered occlusion analysis in depth.

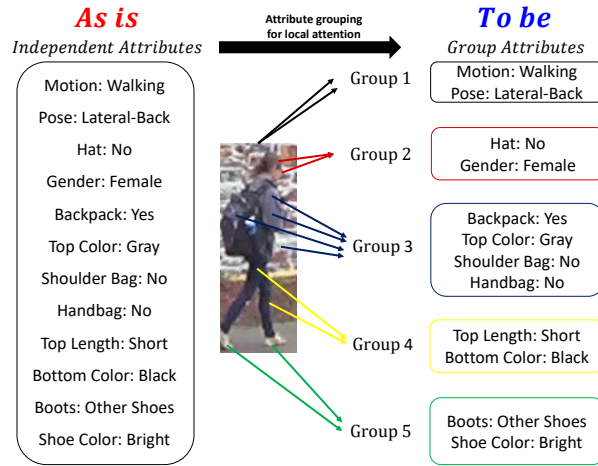


Figure 1: Attribute grouping for local attention. Physically adjacent pedestrian attributes are grouped into one group. Group 1 is for attributes related to the entirety of a pedestrian. Groups 2, 3, 4, and 5 are for attributes related to the pedestrian’s head, upper body, lower body, and feet, respectively. The network focuses on the semantic information of the pedestrian so that it can be robust against occluded pedestrians as obstacles.

In this paper, we propose a novel method for improving the PAR performance in occlusion cases.

As an intuitive idea, to avoid attending the frame with occlusion, we select the frame that can best estimate each attribute. Therefore, one solution involves the use of sparsity regularization [11] of the temporal weights. In other words, sparse attention takes full advantage of the meaningful information in the other weighted frames. However, unfortunately, our experiment results showed that adding this simple sparsity constraint to the method in [10] cannot correctly handle occlusion. This is because the method proposed in [10] uses multiple independent branches for multi-attribute classification. On the other hand, pedestrian attributes are closely related to each other. In particular, semantically adjacent attributes have more significant relationships, as depicted in Figure 1. However,

sparsity-constrained temporal attention cannot understand the relationships between the attributes either. Therefore, the relationship between attributes is key to finding meaningless frames, and we formulate it as a group sparsity-based temporal attention.

Group sparsity [12] is an advanced method compared to sparsity; it can gather the related attention of the attributes into a group. For instance, in Figure 1, information regarding the boots and shoe color is destroyed at the same time an obstacle occludes a pedestrian’s feet. In this case, group sparsity puts the boots and shoe color into one group. Then, their attention weights are simultaneously suppressed. Therefore, the group constraint achieves more robust results for occlusion situations than those of the sparsity method. Figure 2 represents an overview of the proposed method, which consists of a shared feature extractor, multiple attribute classification branches, and a group sparsity-based attention across multiple branches. Extensive experiments were conducted to demonstrate the robustness of the proposed method to occlusion. The proposed method achieved a higher F_1 -score than that of the state-of-the-art methods on occlusion samples based on the DukeMTMC-VideoReID [10, 13, 14] and MARS [10, 15] benchmark datasets. In addition, the proposed method was carefully validated on five occlusion scenarios and its results were consistently better than those of the baselines.

Our main contributions are summarized as follows.

- The proposed temporal attention module is designed to reflect the temporal sparsity of useful frames in a crowded video. Our model is guided to not pay attention to the occluded frame, but rather to the frame where relevant

attributes are visible.

- When a pedestrian is occluded owing to obstacles, information on several related attributes is difficult to infer simultaneously. Therefore, we propose a novel group sparsity-based temporal attention module. This module allows a model to robustly pay attention to meaningful frames to recognize the group attributes of a pedestrian.
- Extensive experiments showed that the proposed method outperformed the state-of-the-art methods on two video-based PAR datasets, especially for occlusion samples. We also confirmed that the results were consistently better than those of the baselines on the five occlusion scenarios.

The remainder of this paper is organized as follows. We first introduce some related work in Section 2. The proposed method is described in Section 3. Section 4 presents the implementation details and experimental results. Finally, we conclude the paper in Section 5.

2. Related Works

2.1. Pedestrian Attribute Recognition

Studies have been conducted on image-based PAR using various methods [2, 3, 6, 16]. Liu *et al.* [2] proposed the HydraPlus-Net network that utilizes multi-scale features. Zhao *et al.* [3] proposed a recurrent convolutional architecture that understands the relationships between each group for PAR. Siadari *et al.* [6]

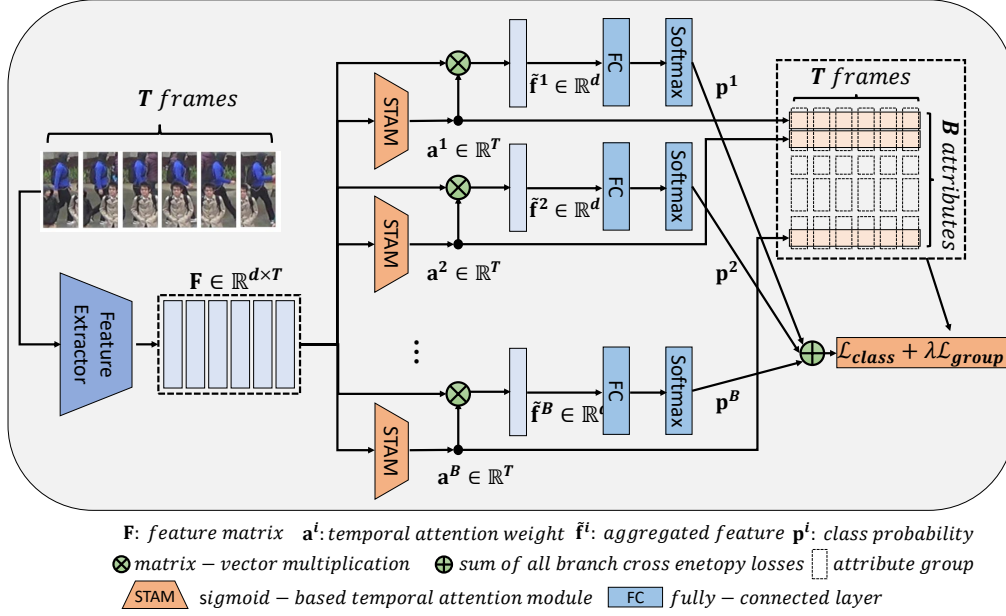


Figure 2: Overview of the network architecture of the proposed method. It consists of a feature extractor, sigmoid-based temporal attention modules, and attribute classifiers. Because the attributes of the pedestrians are closely related to each other, the attention weights for semantically adjacent attributes have similar values to each other. In other words, temporal frame attentions are not independent. To reflect this point, we formulate a group sparsity-based temporal attention module constraint.

utilized a global super-resolution network for resolving low-resolution problems and a multi-attribute recognition.

Accurate attribute recognition for various environments such as occlusion situations is difficult to achieve with image-based PAR. A video has more information than that of an image; thus, the number of video-based studies has been increasing. Chen *et al.* [10] proposed an attention module that indicates the extent to which the model pays attention to each frame for each attribute. They designed branches and classifiers for each attribute in the video. Specker *et al.* [17] used global features before temporal pooling to utilize the different pieces of informa-

tion from various frames. However, existing video-based PAR methods have not yet considered occlusion problem in depth. In this paper, we focus on the occlusion handling of video-based PAR.

2.2. Sparsity Loss

The sparsity regularization is often used for selection problems [18, 19, 20, 21]. Nguyen *et al.* [18] proposed a sparse temporal pooling network for action localization in a video. In this method, the sparsity loss makes the model select the segments that are related to the target action. Islam *et al.* [19] proposed a hybrid attention mechanism network consisting of soft, semi-soft, and hard attention modules. The sparsity loss is designed using the ℓ_1 norm of the attention scores from the soft attention module; this causes the network to select segments sparsely. Luo *et al.* [21] proposed the Action Unit Memory Network. In the process of updating the templates in the memory bank, the foreground attention weights are used with the ℓ_1 sparsity loss to alleviate the interference from the background segments.

Unlike the sparsity loss method that adjusts each value, the group sparsity loss method simultaneously controls the values associated with each other [22, 23, 24, 25, 26, 27]. We propose a method that adjusts the attention weights of pedestrian attributes at the same time by designing the group sparsity constraint.

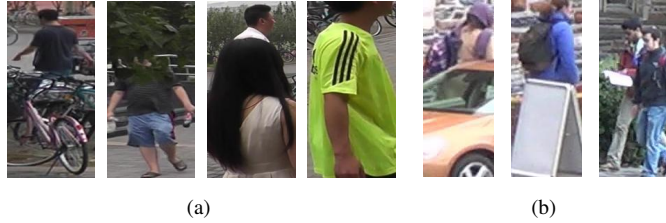


Figure 3: (a) and (b) represent the occlusion types in MARS and DukeMTMC-VideoReID datasets, respectively. There are various occlusion types, such as a pedestrian’s lower body or head, other pedestrians, and tracking failure.

3. Proposed Method

3.1. Problem Formulation

Figure 3 shows examples of occluded pedestrian images from two video PAR datasets (DukeMTMC-VideoReID and MARS [10]). Typically, pedestrian images obtained from surveillance cameras in the real world are often obscured by crowded people, cars, and buildings. In addition, the instability of pedestrian tracking results in distorted pedestrian images. Therefore, it is important to robustly recognize the pedestrian attributes in occlusion situations; however, occluded pedestrian images make a single image-based PAR impossible. This study aims to achieve robust PAR using multiple frames, *i.e.*, video-based PAR.

3.2. Overview

The proposed method consists of a feature extractor, attention modules, and attribute classifiers, and the inputs are a set of T frames, as depicted in Figure 2. First, any feature extraction networks can be used. Here, we use the same feature extractor as that used in our baselines [10], which consists of a ResNet [28] and two convolution modules to extract two types of feature according to their

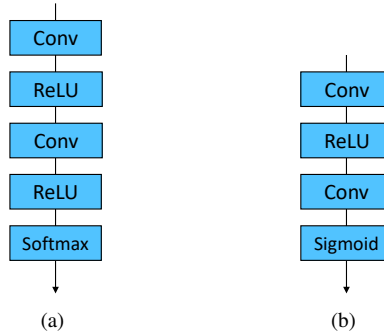


Figure 4: (a) Softmax-based probabilistic temporal attention module (*PTAM*) proposed by Chen *et al.* [10]; (b) sigmoid-based temporal attention module (*STAM*) of the proposed method.

relevance to the identification (for more details, please see [10]). Second, a novel attention model is proposed to aggregate multiple features from T frames in which attention weights are constrained by the temporal sparsity of frames and the group sparsity of pedestrian attributes. Finally, multi-branch classifiers are used for multi-labeled attribute classifications (*e.g.*, hat, backpack, shoe type, and color). Notably, unlike the existing work [10], which trains multiple attribute classifiers using independent classification loss only, the proposed method trains multiple classifiers using feature vectors constrained by a group sparsity-based temporal attention module. In the following sections, we will explain the novel group sparsity-based temporal attention module.

3.3. Temporal Attention Module-Based Classification

The body parts of a pedestrian are often occluded owing to obstacles and other pedestrians in real-world videos. Therefore, the information needed to recognize pedestrian attributes is different for each frame, even in the same video. For example, when there is a frame in which all parts of a pedestrian are visible and

a frame in which an obstacle obscures the pedestrian’s lower body, the amount of information on the lower body provided by each frame is different. We compute the temporal attention weights for T frames to utilize the different pieces of information from each frame.

Chen *et al.* [10] designed the temporal attention as a softmax-based probabilistic temporal attention module (*PTAM*) that calculates important probabilities for frames in the temporal direction, as depicted in Figure 4a. However, in the last ReLU-Softmax in Figure 4a, ReLU [29] converts all the negative values to zero and softmax normalizes the sum of the attention weights of the T frame equal to 1. This makes it difficult to obtain attention weights that reflect sparsity constraints [18]. In other words, if the weight of a particular frame becomes 1, the weight of the rest of the frame becomes 0. To solve this issue, we designed a sigmoid-based temporal attention module (*STAM*) configured with Conv-ReLU-Conv-Sigmoid, as depicted in Figure 4b. The sigmoid after Conv allows any frame to have a weight close to 0 or 1.

A temporal attention weight vector for the i -th attribute type, $\mathbf{a}^i \in \mathbb{R}^T$, can be obtained as

$$\mathbf{a}^i = STAM^i(\mathbf{F}), \quad (1)$$

where $STAM^i(\cdot)$ is a sigmoid-based temporal attention module for the i -th attribute and $\mathbf{F} = [\mathbf{f}_1, \mathbf{f}_2, \dots, \mathbf{f}_T] \in \mathbb{R}^{d \times T}$ is a feature matrix that contains a set of d -dimensional feature vectors corresponding to T frames, which is obtained from the same feature extractor as used in [10]. Finally, an aggregated feature vector

for the i -th attitude classification, $\tilde{\mathbf{f}}^i \in \mathbb{R}^d$, is obtained by multiplying the feature matrix \mathbf{F} and the attention weight vector \mathbf{a}^i as

$$\tilde{\mathbf{f}}^i = \mathbf{F}\mathbf{a}^i = \sum_{t=1}^T a_t^i \cdot \mathbf{f}_t. \quad (2)$$

Then, we pass $\tilde{\mathbf{f}}^i$ to the i -th linear attribute classifier and return a prediction vector \mathbf{p}^i for each attribute.

$$\mathbf{p}^i = \text{Softmax}(\mathbf{W}^i \tilde{\mathbf{f}}^i), \quad (3)$$

where $\text{Softmax}(\cdot)$ is a softmax function, $\mathbf{W}^i \in \mathbb{R}^{c \times d}$ is a weight matrix of a fully connected layer for the i -th attribute classification branch, and c is the number of classes of the branch. The classification loss \mathcal{L}_{class} is the sum of the cross-entropy (CE) [30] of the attributes.

$$\mathcal{L}_{class} = \sum_{i=1}^B \beta^i CE(\mathbf{p}^i), \quad (4)$$

where B is the number of branches for each attribute in Figure 2. β^i is a balancing hyperparameter for the i -th attribute classification. It is set as a reciprocal of the number of classes in each attribute because each attribute classification has a different number of classes.

3.4. Limitation of Sparsity Constraint on STAM

The temporal attention weight \mathbf{a}^i in Equation (2) is an indicator that represents the importance of each frame. The sparsity constraint for the attention weight

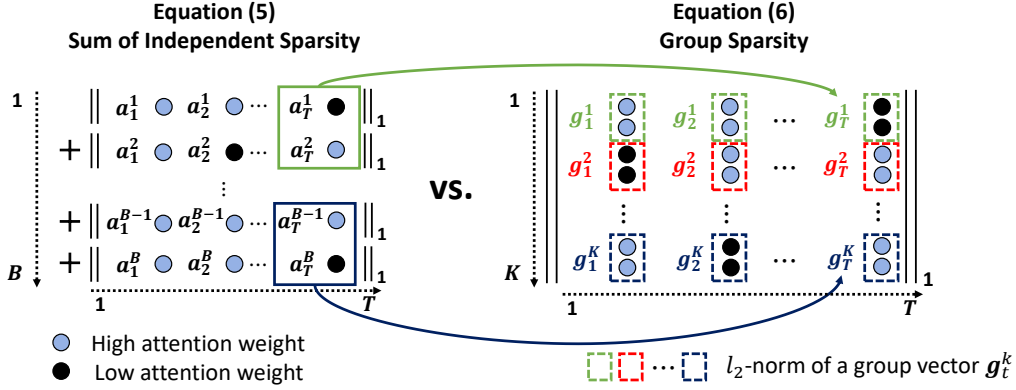


Figure 5: Comparison between the sparsity- and the group sparsity-based constraints. Unlike the sparsity-based method, which adjusts each value independently, the group sparsity-based method simultaneously controls the values associated with each other.

further emphasizes the effect and can be computed by the l_1 -norm on \mathbf{a}^i .

$$\mathcal{L}_{sparsity} = \sum_{i=1}^B \|\mathbf{a}^i\|_1, \quad (5)$$

where B is the number of branches of each attribute. Namely, the sparsity loss is the operation of the l_1 norm per branch of each attribute. From the formulation, the sparsity constraint is expected to have the effect of selecting frames that are not occluded from T frames independently for each branch.

However, our experimental results presented in Section 4 indicate that the sparsity constraint on the *STAM* fails to make the correct frame importance, thereby degrading the PAR performance sometimes, as compared with the baselines.

Why does the sparsity constraint not improve the overall performance?

As depicted on the left-hand side of Figure 5, the sparsity constraint on *STAM* is applied to the temporal attention weights by the ℓ_1 norm, independently for each branch; thus, the attention weights of each branch depend only on the temporal information in each attribute. That is, the sparsity constraint does not help a model understand the relations between each attribute. However, pedestrian attributes are closely related to each other. As depicted in Figure 3, information about some attributes such as the type and color of the bottom and the type and color of shoe is damaged simultaneously if a pedestrian’s lower body or feet are occluded. Therefore, another constraint is needed to guide a model to understand the relationship between pedestrian attributes, which is important for achieving an algorithm that is robust to occlusion situations. In the next section, we design the attribute relations as attribute groups and formulate the group constraints of attributes.

3.5. Group Sparsity Constraint on *STAM*

Group sparsity extends and generalizes how to learn sparsity regularization, by which prior assumptions on the structure of the input variables can be incorporated [12, 31]. For the occluded pedestrian’s attributes, the prior assumption is that pedestrian attributes can be partitioned into K groups on the basis of their relevance, *i.e.*, \mathcal{G}^k where $k = 1, 2, \dots, K$, as depicted in Figure 1. As a result, the attention weights in the same group at time t , $\{a_t^i | i \in \mathcal{G}^k\}$, can be constrained by

considering the group structure.

The method for grouping multiple attribute weights at time t involves introducing a new vector at time t using each attribute group, *i.e.*, $\mathbf{g}_t^k \in \mathbb{R}^{|\mathcal{G}^k|}$, as depicted on the right-hand side of Figure 5. By computing the ℓ_2 norm of a group vector \mathbf{g}_t^k , we can define two sparsity constraints on attributes and time as

$$\mathcal{L}_{group} = \sum_{t=1}^T \sum_{k=1}^K \gamma_k \|\mathbf{g}_t^k\|_2, \quad (6)$$

where $\|\mathbf{g}_t^k\|_2$ always has positive values and, thus the sum of these values is equal to the ℓ_1 norm. γ_k is a balancing hyperparameter for the k -th group in the sum of all the group sparsity loss functions. It is set as a reciprocal of the number of attributes in each group because each group has a different number of attributes.

The \mathcal{L}_{group} constraint on *STAM* simultaneously increases or decreases the attention weights of specific groups in particular frames. It helps a model understand which frames are more important for each group and which groups in the same frame are recognizable. This constraint is consistent with the prior assumption that groups exist between attributes. In addition, it does not use explicit local patches in frames for specific attribute recognition. It uses implicit attention by attribute groups, enabling robust attribute recognition for pedestrian appearance distortions due to tracking failures.

Finally, the total loss function consists of \mathcal{L}_{class} and \mathcal{L}_{group} described above, as follows:

$$\mathcal{L}_{total} = \mathcal{L}_{class} + \lambda \mathcal{L}_{group}. \quad (7)$$

Table 1: The attribute groups for DukeMTMC-VideoReID and MARS datasets.

Group	DukeMTMC-VideoREID	MARS
Whole	motion, pose	motion, pose
Head	hat, gender	age, hat, hair, gender
Upper Body	backpack, top color, shoulder bag, handbag	backpack, top color, shoulder bag, handbag, top length
Lower Body	top length, bottom color	bottom length, bottom color, type of bottom
Foot	boots, shoe color	-

where λ is a weight factor that combines the classification loss and the group sparsity loss.

4. Experiments

4.1. Implementation Details

Tables 1 show the attribute groups of the group sparsity for the experiments. We used the same feature extractor as [10], which is pre-trained on the ImageNet dataset [32]. The initial learning rate was set to $3e-4$ and multiplied by 0.3 at 100 epochs. The weight decay was set to $5e-4$ for the Adam optimizer [33]. For the input, the width and height of the frame were resized to 112 and 224, respectively. The weight factor λ in Equation 7 was set to 0.02. The batch size for training was set to 64. The model was trained for 200 epochs, and the best results were reported among the measurements every 20 epochs. The sequence length T of the frames for training was set to six according to what was done in a previous work [10]. In the test phase, we divided the trajectory of a pedestrian into segments consisting

of six frames. The divided segments were independently inferred, and the results were averaged for PAR. In other words, the performance was measured using one prediction per trajectory as done in [10]. We used a single NVIDIA Titan RTX GPU for both the training and the inference. Regarding our experimental setting, if no additional explanation is given, we follow the process detailed in the baselines [10] for a fair comparison.

4.2. Evaluation and Datasets

We evaluated the proposed method using the average accuracy and F_1 -score and compared it with three baselines: Chen *et al.* [10], 3D-CNN [34], and CNN-RNN [35]. 3D-CNN and CNN-RNN are the same methods used in [10]. For a fair comparison, the random seed for the experiments was fixed deterministically and trained the three baselines using the released codes.

For the extensive experiments, we used two video-based PAR datasets: DukeMTMC-VideoReID and MARS [10], which were derived from the re-identification datasets, DukeMTMC-VideoReID [13] and MARS [15], respectively. Chen *et al.* [10] re-annotated them for the video-based PAR datasets.

4.2.1. DukeMTMC-VideoReID Dataset

The DukeMTMC-VideoReID dataset contains 12 types of pedestrian attribute annotations. The eight attributes are binary types.¹ The other four attributes are multi-class types.² The attributes were annotated per trajectory, and the total num-

¹backpack , shoulder bag, handbag, boots, gender, hat, shoe color, and top length.

²motion, pose, bottom color, and top color.

Table 2: Comparisons of the results for the total samples of the DukeMTMC-VideoReID and MARS datasets.

Dataset	Method	Average Accuracy (%)	Average F_1 -score (%)
DukeMTMC-VideoReID	Chen <i>et al.</i> [10]	89.12	71.58
	3DCNN [34]	85.38	64.66
	CNN-RNN [35]	88.80	71.73
	Ours	88.98	72.30
MARS	Chen <i>et al.</i> [10]	86.42	69.92
	3DCNN [34]	81.96	60.39
	CNN-RNN [35]	86.49	69.89
	Ours	86.75	70.42

ber of trajectories was 4832. We excluded four trajectories with fewer frames than the segment length T , and the remaining 4832 trajectories were used in the experiments. For the training, 2195 trajectories were used, 413 of which contained occlusions, as shown in Figure 3b. For the test, 2633 trajectories were used, 449 of which contained occlusions. The average length of the trajectories was approximately 169 frames.

4.2.2. MARS Dataset

The MARS dataset contains 14 types of pedestrian attribute annotations. The ten attributes are binary types³ The other four attributes are multi-class types.⁴ The attributes were also annotated per trajectory, and the total number of trajectories was 16,360. We also excluded five trajectories with fewer frames than the seg-

³shoulder bag, gender, hair, bottom type, bottom length, top length, backpack, age, hat, and handbag.

⁴motion, pose, top color, and bottom color.

Table 3: Comparisons of the results for the occlusion samples of the DukeMTMC-VideoReID and MARS datasets.

Dataset	Method	Average Accuracy (%)	Average F_1 -score (%)
DukeMTMC-VideoReID	Chen <i>et al.</i> [10]	88.33	69.03
	3DCNN [34]	84.41	61.38
	CNN-RNN [35]	87.94	68.12
	Ours	88.36	70.21
MARS	Chen <i>et al.</i> [10]	66.39	55.67
	3DCNN [34]	60.83	46.16
	CNN-RNN [35]	65.83	53.79
	Ours	71.94	61.88

ment length T , and the remaining trajectories were 16,355. For the training, 8297 trajectories were used, 35 of which contained occlusions, as shown in Figure 3a. For the test, 8058 trajectories were used, 30 of which contained occlusions. The average length of the trajectories was about 60 frames.

4.3. Evaluation on the DukeMTMC-VideoReID and MARS Datasets

Table 2 shows the performances of the methods on the total samples of the DukeMTMC-VideoReID and MARS datasets, where the proposed method outperformed the baselines. Only in one case in the DukeMTMC-VideoReID dataset did the Chen *et al.* [10] method show slightly better average accuracy. However, because the measure of average accuracy did not consider data imbalance, the difference was negligible. In addition, Table 2 does not correctly show the performances on the occlusion samples because the percentage of such samples among the total samples was very low. To evaluate the robustness of the proposed

Table 4: Comparisons of the attribute-wise average F_1 -scores (%) for the occlusion samples of the DukeMTMC-VideoReID dataset.

Attributes	Chen <i>et al.</i> [10]	3DCNN [34]	CNN-RNN [35]	Ours
motion	24.80	24.78	24.80	24.80
pose	67.87	63.48	65.44	65.00
bottom color	46.39	34.70	41.17	51.49
top color	51.65	45.07	52.30	52.81
handbag	59.09	53.97	55.03	60.39
top length	78.44	72.79	76.06	80.82
shoe color	78.56	60.24	77.84	81.13
hat	88.59	78.10	85.60	88.46
shoulder bag	70.95	65.62	73.83	73.61
boots	89.82	79.27	92.31	90.01
backpack	85.35	79.55	85.30	86.67
gender	86.81	79.00	87.73	87.31
average	69.03	61.38	68.12	70.21

method in occlusion situations, we compared its performance using only the occlusion samples with those of the baselines. Table 3 presents the results on the DukeMTMC-VideoReID and MARS datasets. To ensure accurate evaluations, we excluded the hat and handbag attributes of the MARS dataset because the ground truth of both attributes for all occlusion samples was the same, *i.e.*, “no.” As shown in Table 3, the proposed method outperformed the baselines in all cases and achieved average accuracies of 88.36% and 71.94%, and average F_1 -scores of 70.21% and 61.88% on the occlusion samples of the DukeMTMC-VideoReID and MARS datasets, respectively.

Tables 4 and 5 present the F_1 -score per attribute on the occlusion samples of the DukeMTMC-VideoReID and MARS datasets, respectively. The proposed

Table 5: Comparisons of the attribute-wise average F_1 -scores (%) for the occlusion samples of the MARS dataset.

Attributes	Chen <i>et al.</i> [10]	3DCNN [34]	CNN-RNN [35]	Ours
motion	44.10	76.00	36.17	44.10
pose	25.52	34.05	40.56	44.31
shoulder bag	54.86	40.34	40.34	54.86
gender	59.71	34.53	72.85	74.36
hair	75.32	47.50	66.52	85.00
bottom type	47.92	37.50	53.42	47.92
bottom length	92.06	81.69	96.15	92.50
top length	41.18	41.18	41.18	91.48
backpack	80.39	41.18	85.58	88.00
top color	32.99	33.03	25.83	22.04
bottom color	49.90	46.92	35.82	45.85
age	64.11	40.00	51.11	52.10
average	55.67	46.16	53.79	61.88

method showed a performance similar to or better than those of the baselines for all attributes, except for the pose attribute. In particular, Table 4 shows that the F_1 -score of the proposed method for the bottom color attribute was 5.1% higher than that of the Chen *et al.* [10] method. This is because the lower body of the pedestrians in the DukeMTMC-VideoReID dataset is often obscured by objects such as cars. In addition, the lower body must be visible to recognize the top-length attribute. As a result, Table 4 shows that the proposed method achieved the best F_1 -score for the top-length attribute, with a 2.38% improvement over the second-best method.

On the occlusion samples of the MARS dataset, the proposed method achieved a significant improvement, as shown in Table 5. In particular, for the gender, hair,

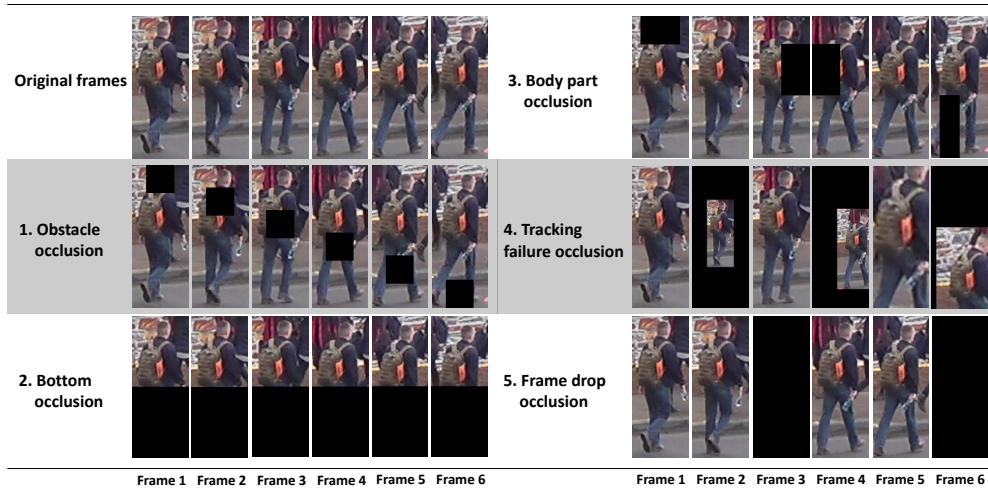


Figure 6: Examples of the five occlusion scenarios.

and pose attributes, the improvements in the F_1 -score were 18.79%, 14.65%, and 9.68%, respectively. The reason why these three attributes greatly improved is that the MARS dataset includes tracking failure cases where some pedestrian body parts lie outside the frames, as shown in Figure 3a. In other words, the proposed group sparsity-constrained STAM is designed to implicitly pay attention to space and time, leading to the robustness of the tracking failure. Robustness of the proposed method to upper body occlusion was also demonstrated, achieving 8.49% and 50.3% improvements for the backpack and top length attributes, respectively, compared to those of the Chen *et al.* [10] method.

4.4. Evaluation on Various Occlusion Scenarios

The DukeMTMC-VideoReID and MARS datasets contain 449 and 30 occlusions for the testing samples, respectively. These are not sufficient to measure accurate performance in occlusion situations. We designed five synthetic occlu-

Table 6: Comparisons of the average F_1 -scores (%) for the obstacle occlusion scenario of the DukeMTMC-VideoReID and MARS datasets.

Dataset	Occlusion probability (p)	Chen <i>et al.</i> [10]	3DCNN [34]	CNN-RNN [35]	Ours
DukeMTMC-VideoReID	0.0	71.58	64.66	71.73	72.30
	0.3	71.24	64.38	70.93	72.18
	0.5	70.85	63.36	70.49	72.04
	0.7	70.56	62.15	69.93	71.75
	1.0	69.35	58.64	68.78	70.14
MARS	0.0	69.92	60.39	69.89	70.42
	0.3	69.78	59.64	69.28	70.26
	0.5	69.60	58.35	68.12	70.11
	0.7	69.45	57.31	67.12	69.99
	1.0	68.88	54.10	63.85	69.29

sion scenarios, as depicted in Figure 6, to analyze the robustness of the proposed method in various occlusion situations. The number of synthesized test samples for each scenario was 2633 and 8058 for the DukeMTMC-VideoReID and MARS datasets, respectively, which are the same as the total number of test samples in the original datasets. Notably, we did not retrain the proposed method and baseline methods to prevent the models from learning the tendency of synthetic occlusion.

The first scenario is an obstacle occlusion, in which pedestrians are occluded by an obstacle sequentially from the head to feet. We randomly selected segments with the probability p in a trajectory and generated an occlusion of the selected segments. We conducted experiments using different values of p . The second scenario is the bottom occlusion scenario, which simulates the situation in which cars and bicycles pass through and occlude the pedestrian’s lower body. We randomly selected segments, as in the first scenario. The third scenario is a body part occlusion. In this scenario, a pedestrian’s head, left and right sides of the up-

Table 7: Comparisons of the average F_1 -scores (%) for the bottom occlusion scenario of the DukeMTMC-VideoReID and MARS datasets.

Dataset	Occlusion probability (p)	Chen <i>et al.</i> [10]	3DCNN [34]	CNN-RNN [35]	Ours
DukeMTMC-VideoReID	0.0	71.58	64.66	71.73	72.30
	0.3	70.46	61.94	70.94	71.78
	0.5	68.80	57.79	69.50	70.56
	0.7	66.77	53.16	67.42	68.29
MARS	0.0	69.92	60.39	69.89	70.42
	0.3	68.95	58.69	69.30	69.84
	0.5	67.18	54.69	67.85	68.59
	0.7	65.57	52.12	66.35	66.81

per body, and left and right sides of the lower body are randomly occluded. The probability of occlusion in each frame was set by a Bernoulli distribution with a parameter of 0.5, and one body part was randomly occluded in the selected frame. The fourth scenario is a tracking failure, in which a pedestrian is randomly translated or zoomed, *i.e.*, affine transformed⁵. Finally, the fifth scenario is the frame drop. We randomly selected frames similar to the cases of the second and third scenarios, and filled the selected frames with zero values, *i.e.*, black.

Tables 6 and 7 show the average F_1 -scores on the first and second scenario samples of the DukeMTMC-VideoReID and MARS datasets, and as can be seen, the proposed method consistently achieved better results in comparison to those of the baselines as the probability of occlusion increased. Table 8 presents the average F_1 -scores for the obstacle ($p = 0.5$), bottom ($p = 0.5$), body part, tracking failure, frame drop, and bottom occlusion scenarios. In all the cases, the proposed

⁵The range of translation error is within 30% of the image size on both datasets. The range of a scale is within 25% and 50% on the DukeMTMC-VideoReID and MARS datasets, respectively.

Table 8: Comparisons of the average F_1 -scores (%) for the five occlusion scenarios of the DukeMTMC-VideoReID and MARS datasets.

Dataset	Type	Chen <i>et al.</i> [10]	3DCNN [34]	CNN-RNN [35]	Ours
DukeMTMC-VideoReID	Obstacle ($p = 0.5$)	70.85	63.36	70.49	72.04
	Bottom ($p = 0.5$)	68.80	57.79	69.50	70.56
	Body part	71.02	62.33	70.01	72.11
	Tracking failure	69.82	50.44	70.06	71.73
	Frame drop	70.68	47.58	70.01	71.69
MARS	Obstacle ($p = 0.5$)	69.60	58.35	68.12	70.11
	Bottom ($p = 0.5$)	67.18	54.69	67.85	68.59
	Body part	68.65	55.38	67.93	69.08
	Tracking failure	67.73	45.34	67.77	68.27
	Frame drop	68.25	39.59	67.99	68.43

method achieved better performance than those of the baseline methods. The experiment results demonstrated that the proposed method is robust to occlusions, regardless of the scenario.

4.5. Ablation Study

4.5.1. Effects of the Weight Factor λ

We compared the experimental results according to the weight factor λ in Equation 7. The weight factor λ is a parameter that adjusts the sparsity. As shown in Table 9, the proposed method shows higher F_1 -scores than those of the baseline methods, regardless of λ values and the best results were obtained with $\lambda = 0.02$.

4.5.2. Comparisons Between PTAM and STAM

Table 10 shows that the sparsity has the worst performance in terms of both accuracy and F_1 -scores. As explained in Section 3.4, the sparsity constraint cannot help a model understand the relationship between attributes. However, the proposed method using the group sparsity-constrained STAM, which understands the

Table 9: Analysis of the group sparsity loss for the occlusion samples of the DukeMTMC-VideoReID and MARS datasets.

Dataset	Method	Average Accuracy (%)	Average F_1 -score (%)
DukeMTMC-VideoReID	Chen <i>et al.</i> [10]	88.33	69.03
	$\lambda = 0.005$	88.38	69.85
	$\lambda = 0.03$	88.16	69.62
	$\lambda = 0.02$	88.36	70.21
MARS	Chen <i>et al.</i> [10]	66.39	55.67
	$\lambda = 0.005$	68.06	55.07
	$\lambda = 0.03$	70.00	58.89
	$\lambda = 0.02$	71.94	61.88

relationship between each attribute, showed the best performance compared to the other methods. Table 10 and 11 present comparisons between the group sparsity-constrained PTAM and the group sparsity-constrained STAM for the five occlusion scenarios. The group sparsity-constrained STAM outperformed the group sparsity-constrained PTAM in all the occlusion scenarios.

4.6. Qualitative Results

We visualized the temporal attention weight vector with various segment frames to analyze the proposed method’s robustness to occlusion situations. Figure 7 presents the temporal attention vectors and the PAR results of the method presented by Chen *et al.* [10] and that of our method for all the groups of the DukeMTMC-VideoReID dataset. The values of the baseline method have similar values in all the frames. In contrast, the values of the proposed method have different values in each frame. Moreover, the values of the occlusion frames are

Table 10: Comparisons between the sparsity-based and the group sparsity-based (ours) constraints for the occlusion samples of the DukeMTMC-VideoReID and MARS datasets.

Dataset	Method	Softmax	Sigmoid	Total samples		Occlusion samples	
				Average Accuracy (%)	Average F_1 -score (%)	Average Accuracy (%)	Average F_1 -score (%)
DukeMTMC-VideoReID	Chen <i>et al.</i> [10]	✓	-	89.12	71.58	88.33	69.03
	Sparsity	✓	-	88.50	71.95	87.99	69.05
	Group sparsity	✓	-	88.68	71.92	88.23	70.24
	Chen <i>et al.</i> [10]	-	✓	88.78	71.59	87.94	69.26
	Sparsity	-	✓	88.20	69.36	87.68	67.52
	Group sparsity	-	✓	88.98	72.30	88.36	70.21
MARS	Chen <i>et al.</i> [10]	✓	-	86.42	69.92	66.39	55.67
	Sparsity	✓	-	86.43	69.84	70.00	57.76
	Group sparsity	✓	-	86.50	69.76	71.94	61.70
	Chen <i>et al.</i> [10]	-	✓	86.30	69.77	66.94	55.92
	Sparsity	-	✓	86.32	68.13	69.17	57.80
	Group sparsity	-	✓	86.75	70.42	71.94	61.88

Table 11: Comparisons of the average F_1 -scores (%) for the five occlusion scenarios of the DukeMTMC-VideoReID and MARS datasets.

Dataset	Method	Softmax	Sigmoid	Type of occlusion scenario				
				Obstacle ($p = 0.5$)	Bottom ($p = 0.5$)	Body part	Tracking failure	Frame drop
DukeMTMC-VideoReID	Chen <i>et al.</i> [10]	✓	-	70.85	68.80	71.02	69.82	70.68
	Ours	✓	-	71.23	70.44	71.42	70.46	70.75
	Ours	-	✓	72.04	70.56	72.11	71.73	71.69
MARS	Chen <i>et al.</i> [10]	✓	-	69.60	67.18	68.65	67.73	68.25
	Ours	✓	-	68.05	65.54	67.83	65.33	68.27
	Ours	-	✓	70.11	68.59	69.08	68.27	68.43

lower than those of the general frames. The attention weights of the bottom and top length attributes are simultaneously controlled because they belong to the same group. For the same reason, the attention weights of the shoe color and boot attributes are also simultaneously adjusted. As a result, the baseline method predicted the shoe color attribute different from the ground truth. However, the proposed method accurately predicted all attributes.

Figure 8 shows an example of the temporal attention weights and the PAR

results for the frame drop occlusion scenario of the MARS dataset. In this case, the attention weights of the proposed method tend to be the same in the same group. However, the attention weights of the baseline method are adjusted independently. Even the values of motion, pose, hair, backpacks, and type of bottom attributes are the same in all the frames. Thereby, the baseline method failed to predict the top color attribute. In contrast, the proposed method accurately predicted the top color.

Figure 9 presents more examples of the PAR results for the DukeMTMC-VideoReID and MARS datasets. In these examples, some of the frames are occluded by other objects or distorted. The baseline method failed to accurately predict some attributes, while the proposed method gives accurate results. It demonstrates that the proposed method is robust to occlusion regardless of the occlusion types.

5. Conclusion

This paper proposed a novel group sparsity-constrained temporal attention module to robustly recognize pedestrian attributes in occlusion situations. The proposed method was formulated as a group sparsity to consider the relationship between pedestrian attributes, which improves the temporal attention. The results of extensive experiments demonstrated that the proposed method consistently outperformed all the baselines.

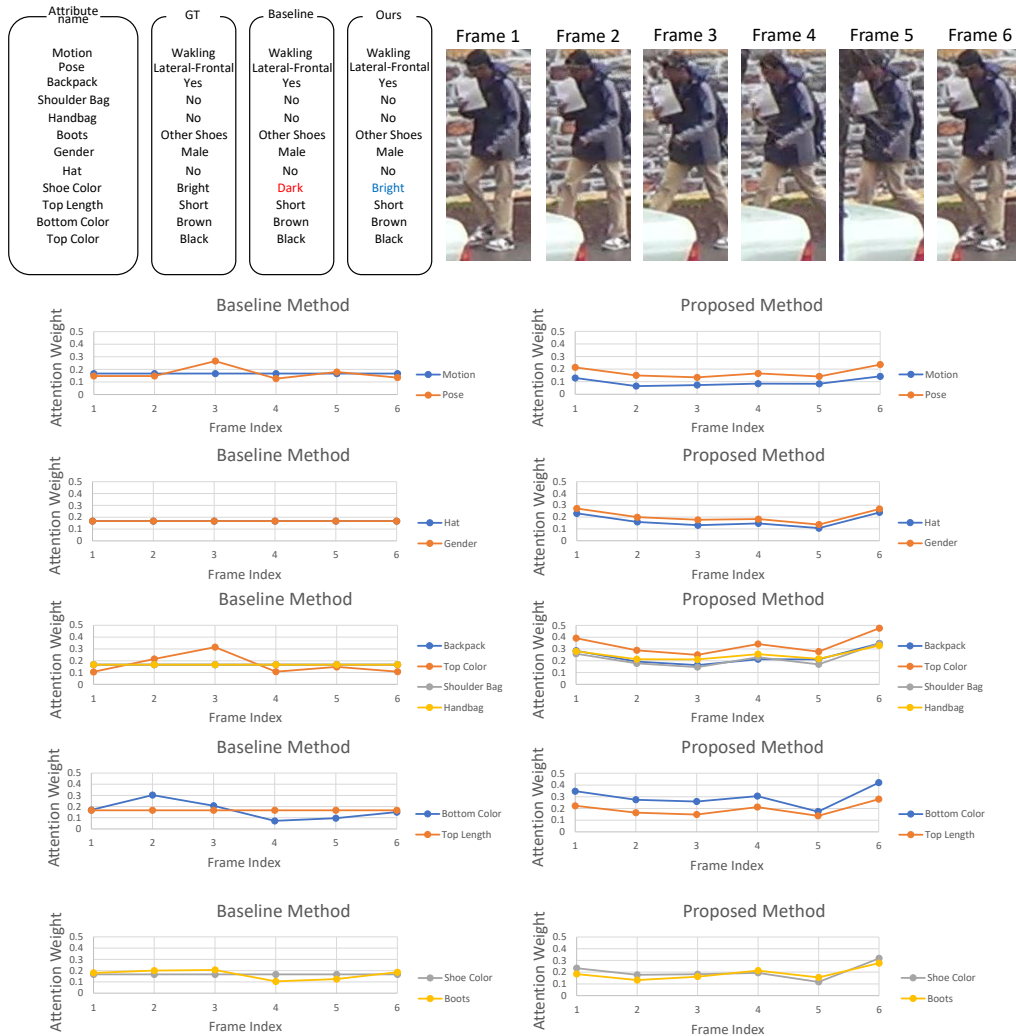


Figure 7: Qualitative results for the DukeMTMC-VideoReID dataset. It shows the attention weights of the group attributes and the PAR results. For the groups related to the lower body, the proposed method has low attention weights in the occluded frames. However, the attention weights of the baseline method (Chen *et al.* [10]) are almost the same in all the frames.

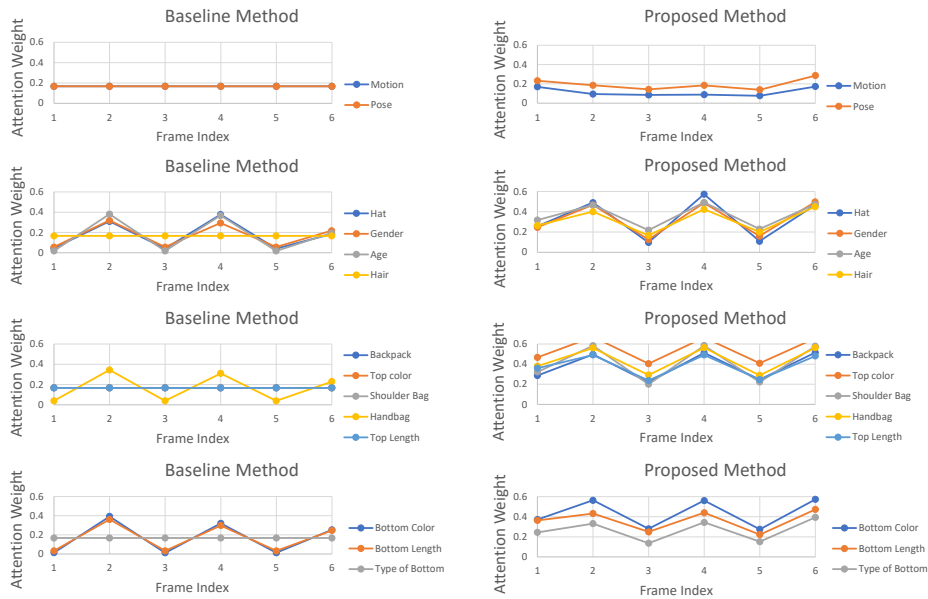
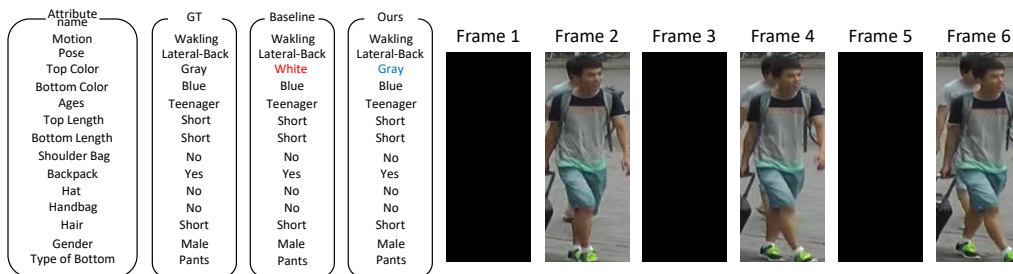


Figure 8: Qualitative results for the frame drop occlusion scenario of the MARS dataset. It shows the attention weights of the group attributes and the PAR results. In the proposed method, the attention weights of most attributes are simultaneously adjusted according to the occluded frames. However, in the baseline method (Chen *et al.* [10]), many attributes such as backpack, top color, and shoulder bag have attention weights even in dropped frames.

Attribute name	GT	Baseline	Ours	Frame 1	Frame 2	Frame 3	Frame 4	Frame 5	Frame 6
Motion	Walking	Walking	Walking						
Pose	Lateral-Back	Lateral-Back	Lateral-Back						
Backpack	No	No	No						
Shoulder Bag	Yes	Yes	Yes						
Handbag	No	No	No						
Boots	No	No	No						
Gender	Female	Female	Female						
Hat	Yes	Yes	Yes						
Shoe Color	Dark	Dark	Dark						
Top Length	Short	Short	Short						
Bottom Color	Black	Black	Black						
Top Color	Black	Black	Black						

(a) The occlusion samples of the DukeMTMC-VideoReID dataset.

Attribute name	GT	Baseline	Ours	Frame 1	Frame 2	Frame 3	Frame 4	Frame 5	Frame 6
Motion	Walking	Walking	Walking						
Pose	Lateral-Back	Lateral-Back	Lateral-Back						
Top Color	White	White	White						
Bottom Color	Blue	Blue	Blue						
Ages	Teenager	Teenager	Teenager						
Top Length	Short	Short	Short						
Bottom Length	Long	Long	Long						
Shoulder Bag	No	No	No						
Backpack	Yes	Yes	Yes						
Hat	No	No	No						
Handbag	No	No	No						
Hair	Long	Short	Long						
Gender	Female	Female	Female						
Type of Bottom	Pants	Pants	Pants						

(b) The tracking failure samples of the MARS dataset.

Figure 9: Examples of the PAR results. Because of the occluded frames, the baseline method (Chen *et al.* [10]) incorrectly predicted the pedestrian attributes. However, the proposed method is robust against the occluded frames and shows accurate results.

Acknowledgement

This work was partially supported by Institute of Information & Communications Technology Planning & Evaluation (IITP) grant funded by the Korea government (MSIT) (No.2014-3-00123, Development of High Performance Visual BigData Discovery Platform for Large-Scale Realtime Data Analysis) and by the National Research Foundation of Korea (NRF) grant funded by the Korea government (MSIT) (No. NRF-2019R1F1A1058666).

References

- [1] X. Wang, S. Zheng, R. Yang, B. Luo, J. Tang, Pedestrian attribute recognition: A survey, arXiv preprint arXiv:1901.07474 (2019).
- [2] X. Liu, H. Zhao, M. Tian, L. Sheng, J. Shao, S. Yi, J. Yan, X. Wang, Hydraplus-net: Attentive deep features for pedestrian analysis, in: Proc. of the IEEE Int'l Conf. on Computer Vision, 2017.
- [3] X. Zhao, L. Sang, G. Ding, J. Han, N. Di, C. Yan, Recurrent attention model for pedestrian attribute recognition, in: Proc. of the AAAI Conf. on Artificial Intelligence, 2019.
- [4] S. H. I. Xingjian, Z. Chen, H. Wang, D. Y. Yeung, W. K. Wong, W. C. Woo, Convolutional lstm network: A machine learning approach for precipitation nowcasting, in: Proc. of Advances in Neural Information Processing Systems, 2015.
- [5] T. N. Kipf, M. Welling, Semi-supervised classification with graph convolutional networks, arXiv preprint arXiv:1609.02907 (2016).
- [6] T. S. Siadari, M. Han, H. Yoon, Gsr-mar: Global super-resolution for person multi-attribute recognition, in: Proc. of the IEEE Int'l Conf. on Computer Vision Workshops, 2019.
- [7] Y. Li, C. Huang, C. C. Loy, X. Tang, Human attribute recognition by deep hierarchical contexts, in: Proc. of the European Conf. on Computer Vision, 2016.

- [8] K. Han, Y. Wang, H. Shu, C. Liu, C. Xu, C. Xu, Attribute aware pooling for pedestrian attribute recognition, arXiv preprint arXiv:1907.11837 (2019).
- [9] P. Liu, X. Liu, J. Yan, J. Shao, Localization guided learning for pedestrian attribute recognition, arXiv preprint arXiv:1808.09102 (2018).
- [10] Z. Chen, A. Li, Y. Wang, A temporal attentive approach for video-based pedestrian attribute recognition, in: Chinese Conference on Pattern Recognition and Computer Vision, 2019.
- [11] J. H. Friedman, The elements of statistical learning: Data mining, inference, and prediction, 2017.
- [12] M. Yuan, Y. Lin, Model selection and estimation in regression with grouped variables, *Journal of the Royal Statistical Society: Series B* 68 (1) (2006) 49–67.
- [13] Y. Wu, Y. Lin, X. Dong, Y. Yan, W. Ouyang, Y. Yang, Exploit the unknown gradually: One-shot video-based person re-identification by stepwise learning, in: Proc. of the IEEE Conf. on Computer Vision and Pattern Recognition, 2018.
- [14] E. Ristani, F. Solera, R. Zou, R. Cucchiara, C. Tomasi, Performance measures and a data set for multi-target, multi-camera tracking, in: Proc. of the European Conf. on Computer Vision, 2016.
- [15] L. Zheng, Z. Bie, Y. Sun, J. Wang, C. Su, S. Wang, Q. Tian, Mars: A video

- benchmark for large-scale person re-identification, in: Proc. of the European Conf. on Computer Vision, 2016.
- [16] Q. Li, X. Zhao, R. He, K. Huang, Visual-semantic graph reasoning for pedestrian attribute recognition, in: Proc. of the AAAI Conf. on Artificial Intelligence, 2019.
- [17] A. Specker, A. Schumann, J. Beyerer, An evaluation of design choices for pedestrian attribute recognition in video, in: Proc. of the IEEE Int'l Conf. on Image Processing, 2020.
- [18] P. Nguyen, T. Liu, G. Prasad, B. Han, Weakly supervised action localization by sparse temporal pooling network, in: Proc. of the IEEE Conf. on Computer Vision and Pattern Recognition, 2018.
- [19] A. Islam, C. Long, R. Radke, A hybrid attention mechanism for weakly-supervised temporal action localization, in: Proc. of the AAAI Conf. on Artificial Intelligence, 2021.
- [20] M. Rashid, H. Kjellstrom, Y. J. Lee, Action graphs: Weakly-supervised action localization with graph convolution networks, in: Proc. of the IEEE Winter Conf. on Applications of Computer Vision, 2020.
- [21] W. Luo, T. Zhang, W. Yang, J. Liu, T. Mei, F. Wu, Y. Zhang, Action unit memory network for weakly supervised temporal action localization, in: Proc. of the IEEE Conf. on Computer Vision and Pattern Recognition, 2021.

- [22] J. Cho, M. Lee, H. J. Chang, S. Oh, Robust action recognition using local motion and group sparsity, *Pattern Recognition* 47 (5) (2014) 1813–1825.
- [23] Z. Gao, H. Zhang, G. P. Xu, Y. B. Xue, A. G. Hauptmann, Multi-view discriminative and structured dictionary learning with group sparsity for human action recognition, *Signal Processing* 112 (1) (2015) 83–97.
- [24] Y. Yang, Y. Yang, Z. Huang, H. T. Shen, F. Nie, Tag localization with spatial correlations and joint group sparsity, in: *Proc. of the IEEE Conf. on Computer Vision and Pattern Recognition*, 2011.
- [25] Y. Yang, Z. Huang, Y. Yang, J. Liu, H. T. Shen, J. Luo, Local image tagging via graph regularized joint group sparsity, *Pattern Recognition* 46 (5) (2013).
- [26] J. Luo, W. Wang, H. Qi, Group sparsity and geometry constrained dictionary learning for action recognition from depth maps, in: *Proc. of the IEEE Int’l Conf. on Computer Vision*, 2013.
- [27] S. Tan, X. Sun, W. Chan, L. Qu, L. Shao, Robust face recognition with kernelized locality-sensitive group sparsity representation, *IEEE Trans. on Image Processing* 26 (10) (2017) 4661–4668.
- [28] K. He, X. Zhang, S. Ren, J. Sun, Deep residual learning for image recognition, in: *Proc. of the IEEE Conf. on Computer Vision and Pattern Recognition*, 2016.
- [29] V. Nair, G. E. Hinton, Rectified linear units improve restricted boltzmann machines, in: *Proc. of the Int’l Conf. on Machine Learning*, 2010.

- [30] I. Goodfellow, Y. Bengio, A. Courville, Deep learning, 2016.
- [31] G. Obozinski, L. Jacob, J.-P. Vert, Group lasso with overlaps: the latent group lasso approach, arXiv preprint arXiv:1110.0413 (2011).
- [32] J. Deng, W. Dong, R. Socher, L. J. Li, K. Li, L. Fei-Fei, Imagenet: A large-scale hierarchical image database, in: Proc. of the IEEE Conf. on Computer Vision and Pattern Recognition, 2009.
- [33] D. P. Kingma, J. Ba, Adam: A method for stochastic optimization, arXiv preprint arXiv:1412.6980 (2014).
- [34] S. Ji, W. Xu, M. Yang, K. Yu, 3d convolutional neural networks for human action recognition, IEEE Trans. on Pattern Analysis and Machine Intelligence 35 (1) (2012) 221–231.
- [35] N. McLaughlin, J. M. Del Rincon, P. Miller, Recurrent convolutional network for video-based person re-identification, in: Proc. of the IEEE Conf. on Computer Vision and Pattern Recognition, 2016.